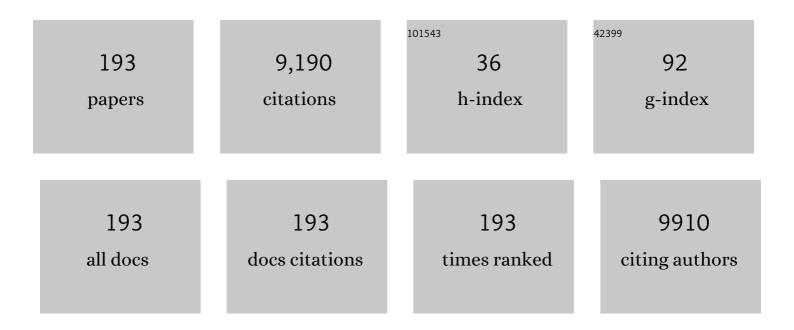
## Sung Heum Park

List of Publications by Year in descending order

Source: https://exaly.com/author-pdf/335716/publications.pdf Version: 2024-02-01



#	Article	IF	CITATIONS
1	Bulk heterojunction solar cells with internal quantum efficiency approaching 100%. Nature Photonics, 2009, 3, 297-302.	31.4	3,903
2	Metallic transport in polyaniline. Nature, 2006, 441, 65-68.	27.8	834
3	Ligand-engineered bandgap stability in mixed-halide perovskite LEDs. Nature, 2021, 591, 72-77.	27.8	471
4	Dual-functional of non-contact thermometry and field emission displays via efficient Bi3+ → Eu3+ energy transfer in emitting-color tunable GdNbO4 phosphors. Chemical Engineering Journal, 2020, 382, 122861.	12.7	173
5	A Thermally Stable Semiconducting Polymer. Advanced Materials, 2010, 22, 1253-1257.	21.0	165
6	Titanium suboxide as an optical spacer in polymer solar cells. Applied Physics Letters, 2009, 95, .	3.3	131
7	Dual-Mode Luminescence with Broad Near UV and Blue Excitation Band from Sr <sub>2</sub> CaMoO <sub>6</sub> :Sm <sup>3+</sup> Phosphor for White LEDs. Journal of Physical Chemistry C, 2015, 119, 15517-15525.	3.1	116
8	Light-soaking issue in polymer solar cells: Photoinduced energy level alignment at the sol-gel processed metal oxide and indium tin oxide interface. Journal of Applied Physics, 2012, 111, .	2.5	112
9	Semiconducting Polymer Photodetectors with Electron and Hole Blocking Layers: High Detectivity in the Near-Infrared. Sensors, 2010, 10, 6488-6496.	3.8	90
10	Novel Filmâ€Casting Method for Highâ€Performance Flexible Polymer Electrodes. Advanced Functional Materials, 2011, 21, 487-493.	14.9	88
11	The design and synthesis of new double perovskite (Na,Li)YMg(W,Mo)O 6 :Eu 3+ red phosphors for white light-emitting diodes. Journal of Alloys and Compounds, 2017, 716, 56-64.	5.5	84
12	Er <sup>3+</sup> -Activated NaLaMgWO <sub>6</sub> double perovskite phosphors and their bifunctional application in solid-state lighting and non-contact optical thermometry. Dalton Transactions, 2019, 48, 4405-4412.	3.3	74
13	Design, Synthesis, and Electroluminescent Property of CNâ^'Poly(dihexylfluorenevinylene) for LEDs. Macromolecules, 2003, 36, 6970-6975.	4.8	71
14	Stabilized Blue Emission from Organic Light-Emitting Diodes Using Poly(2,6-(4,4-bis(2-ethylhexyl)-4H-cyclopenta[def]phenanthrene)). Macromolecules, 2005, 38, 6285-6289.	4.8	70
15	Stabilized Polymers with Novel Indenoindene Backbone against Photodegradation for LEDs and Solar Cells. Macromolecules, 2008, 41, 7296-7305.	4.8	70
16	A low-bandgap alternating copolymer containing the dimethylbenzimidazole moiety. Journal of Materials Chemistry, 2010, 20, 6517.	6.7	68
17	Electroluminescence in polymer-fullerene photovoltaic cells. Applied Physics Letters, 2005, 86, 183502.	3.3	67
18	Novel Electroluminescent Polymers with Fluoro Groups in Vinylene Units. Macromolecules, 2004, 37, 6711-6715.	4.8	63

#	Article	IF	CITATIONS
19	Near-ultraviolet light induced red emission in Sm3+-activated NaSrLa(MoO4)O3 phosphors for solid-state illumination. Journal of Alloys and Compounds, 2020, 817, 152705.	5.5	61
20	Syntheses and properties of electroluminescent polyfluorene-based conjugated polymers, containing oxadiazole and carbazole units as pendants, for LEDs. Polymer, 2005, 46, 12158-12165.	3.8	57
21	Boosting the efficiency of quasi-2D perovskites light-emitting diodes by using encapsulation growth method. Nano Energy, 2021, 80, 105511.	16.0	54
22	A red-emitting perovskite-type SrLa(1â^')MgTaO6:xEu3+ for white LED application. Journal of Luminescence, 2015, 167, 381-385.	3.1	53
23	Improvement of photoluminescence properties of Eu 3+ doped SrNb 2 O 6 phosphor by charge compensation. Optical Materials, 2017, 66, 220-229.	3.6	51
24	Overcoming Fill Factor Reduction in Ternary Polymer Solar Cells by Matching the Highest Occupied Molecular Orbital Energy Levels of Donor Polymers. Advanced Energy Materials, 2018, 8, 1702251.	19.5	48
25	2D Perovskite Seeding Layer for Efficient Airâ€Processable and Stable Planar Perovskite Solar Cells. Advanced Functional Materials, 2020, 30, 2003081.	14.9	48
26	In-situ intramolecular synthesis of tubular carbon nitride S-scheme homojunctions with exceptional in-plane exciton splitting and mechanism insight. Chemical Engineering Journal, 2021, 414, 128802.	12.7	48
27	Achieving non-contact optical thermometer via inherently Eu2+/Eu3+-activated SrAl2Si2O8 phosphors prepared in air. Journal of Alloys and Compounds, 2020, 843, 155858.	5.5	45
28	Tunable single-phased white-emitting Sr 3 Y(PO 4 ) 3 :Dy 3+ phosphors for near-ultraviolet white light-emitting diodes. Ceramics International, 2017, 43, 8497-8501.	4.8	43
29	Isomeric iminofullerenes as acceptors in bulk heterojunction organic solar cells. Journal of Materials Chemistry, 2009, 19, 5624.	6.7	42
30	Controlled crystal facet of MAPbl <sub>3</sub> perovskite for highly efficient and stable solar cell <i>via</i> nucleation modulation. Nanoscale, 2019, 11, 170-177.	5.6	42
31	Single-Crystal-like Perovskite for High-Performance Solar Cells Using the Effective Merged Annealing Method. ACS Applied Materials & Interfaces, 2017, 9, 12382-12390.	8.0	41
32	Highly efficient imide functionalized pyrrolo[3,4-c]pyrrole-1,3-dione-based random copolymer containing thieno[3,4-c]pyrrole-4,6-dione and benzodithiophene for simple structured polymer solar cells. Journal of Materials Chemistry A, 2014, 2, 20126-20132.	10.3	40
33	The role of Yb <sup>3+</sup> concentrations on Er <sup>3+</sup> doped SrLaMgTaO <sub>6</sub> double perovskite phosphors. RSC Advances, 2017, 7, 1464-1470.	3.6	39
34	Understanding and Tailoring Grain Growth of Lead-Halide Perovskite for Solar Cell Application. ACS Applied Materials & Interfaces, 2017, 9, 33925-33933.	8.0	39
35	The tetravalent manganese activated SrLaMgTaO 6 phosphor for w-LED applications. Materials Research Bulletin, 2018, 97, 115-120.	5.2	38
36	Color-Tunable Electroluminescent Polymers by Substitutents on the Poly(p-phenylenevinylene) Derivatives for Light-Emitting Diodes. Chemistry of Materials, 2002, 14, 5090-5097.	6.7	37

#	Article	IF	CITATIONS
37	Eu3+ doped (Li, Na, K) LaMgWO6 red emission phosphors: An example to rational design with theoretical and experimental investigation. Journal of Alloys and Compounds, 2019, 785, 651-659.	5.5	36
38	Low-bandgap poly(4H-cyclopenta[def]phenanthrene) derivatives with 4,7-dithienyl-2,1,3-benzothiadiazole unit for photovoltaic cells. Polymer, 2010, 51, 390-396.	3.8	35
39	Photoluminescence properties, crystal structure and electronic structure of a Sr <sub>2</sub> CaWO <sub>6</sub> :Sm <sup>3+</sup> red phosphor. RSC Advances, 2015, 5, 89290-89298.	3.6	34
40	Crystal structure, electronic structure and photoluminescence properties of KLaMgWO6:Eu3+ phosphors. Journal of Luminescence, 2018, 197, 270-276.	3.1	34
41	Infrared excited Er <sup>3+</sup> /Yb <sup>3+</sup> codoped NaLaMgWO <sub>6</sub> phosphors with intense green up-conversion luminescence and excellent temperature sensing performance. Dalton Transactions, 2019, 48, 11382-11390.	3.3	34
42	Break the Interacting Bridge between Eu3+ Ions in the 3D Network Structure of CdMoO4: Eu3+ Bright Red Emission Phosphor. Scientific Reports, 2018, 8, 5936.	3.3	31
43	Highly crystalline new benzodithiophene–benzothiadiazole copolymer for efficient ternary polymer solar cells with an energy conversion efficiency of over 10%. Journal of Materials Chemistry C, 2018, 6, 4281-4289.	5.5	31
44	Influence of alkaline ions on the luminescent properties of Mn4+-doped MGe4O9 (M = Li2, LiNa and K2) red-emitting phosphors. Journal of Luminescence, 2017, 192, 1072-1083.	3.1	30
45	Blue shift behavior of Eu2+ emission in eulytite-type Sr3La(PO4)3 phosphor based on the release of adjacent Eu3+-induced stress. Journal of Alloys and Compounds, 2018, 742, 159-164.	5.5	30
46	Application of thermally coupled energy levels in Er3+ doped CdMoO4 phosphors: Enhanced solid-state lighting and non-contact thermometry. Materials Research Bulletin, 2019, 117, 63-71.	5.2	28
47	Bilateral Interface Engineering for Efficient and Stable Perovskite Solar Cells Using Phenylethylammonium Iodide. ACS Applied Materials & Interfaces, 2020, 12, 24827-24836.	8.0	27
48	Molybdenum substitution induced luminescence enhancement in Gd2W1-Mo O6:Eu3+ phosphors for near ultraviolet based solid-state lighting. Journal of Luminescence, 2018, 202, 97-106.	3.1	26
49	Oneâ€Pot Exfoliation of Graphitic C <sub>3</sub> N <sub>4</sub> Quantum Dots for Blue QLEDs by Methylamine Intercalation. Small, 2019, 15, e1902735.	10.0	26
50	Simultaneous bifunctional application of solid-state lighting and ratiometric optical thermometer based on double perovskite LiLaMgWO <sub>6</sub> :Er <sup>3+</sup> thermochromic phosphors. RSC Advances, 2019, 9, 7189-7195.	3.6	25
51	Conjugated copolymers based on dihexyl-benzimidazole moiety for organic photovoltaics. Polymer, 2010, 51, 5385-5391.	3.8	24
52	Synthesis and photoluminescence of Bi <sup>3+</sup> ,Eu <sup>3+</sup> doped CdWO <sub>4</sub> phosphors: application of energy level rules of Bi <sup>3+</sup> ions. New Journal of Chemistry, 2016, 40, 3552-3560.	2.8	24
53	Synthesis and characterization of lowâ€bandgap copolymers based on dihexylâ€⊋ <i>hâ€</i> benzimidazole and cyclopentadithiophene. Journal of Polymer Science Part A, 2010, 48, 4567-4573.	2.3	23
54	Syntheses and characterization of carbazole based new lowâ€band gap copolymers containing highly soluble benzimidazole derivatives for solar cell application. Journal of Polymer Science Part A, 2011, 49, 369-380.	2.3	23

#	Article	IF	CITATIONS
55	Eu3+-activated Ca3Mo0.2W0.8O6 red-emitting phosphors: A near-ultraviolet and blue light excitable platform for solid-state lighting and thermometer. Journal of Luminescence, 2020, 223, 117212.	3.1	23
56	Hierarchical multi-level block copolymer patterns by multiple self-assembly. Nanoscale, 2019, 11, 8433-8441.	5.6	22
57	Synthesis and electroluminescent properties of copolymers based on PPV with fluoro groups in vinylene units. Polymer, 2007, 48, 1541-1549.	3.8	21
58	Colloidal GdVO 4 :Eu 3+ @SiO 2 nanocrystals for highly selective and sensitive detection of Cu 2+ ions. Applied Surface Science, 2018, 433, 381-387.	6.1	21
59	Effective hot-air annealing for improving the performance of perovskite solar cells. Solar Energy, 2017, 146, 359-367.	6.1	20
60	Improved Moisture Stability of Perovskite Solar Cells with a Surfaceâ€Treated PCBM Layer. Solar Rrl, 2019, 3, 1800289.	5.8	20
61	Lead Acetate Assisted Interface Engineering for Highly Efficient and Stable Perovskite Solar Cells. ACS Applied Materials & Interfaces, 2020, 12, 7186-7197.	8.0	20
62	Study on Na3Lu1-xEux(PO4)2 phosphor: High efficient Na3Eu(PO4)2 red emitting phosphor with excellent thermal stability. Journal of Alloys and Compounds, 2019, 805, 346-354.	5.5	19
63	Efficiency enhancements in non-fullerene acceptor-based organic solar cells by post-additive soaking. Journal of Materials Chemistry A, 2019, 7, 8805-8810.	10.3	19
64	Solution processable small molecules as efficient electron transport layers in organic optoelectronic devices. Journal of Materials Chemistry A, 2020, 8, 13501-13508.	10.3	19
65	Increased Efficiencies of the Copolymers with Fluoro Groups in Vinylene Units. Macromolecules, 2007, 40, 6799-6806.	4.8	18
66	Tandem Solar Cells Made from Amorphous Silicon and Polymer Bulk Heterojunction Sub ells. Advanced Materials, 2015, 27, 298-302.	21.0	18
67	Synthesis and photovoltaic properties of copolymers with a fluoro quinoxaline unit. Journal of Polymer Science Part A, 2018, 56, 821-830.	2.3	18
68	Open Atmosphere-Processed Stable Perovskite Solar Cells Using Molecular Engineered, Dopant-Free, Highly Hydrophobic Polymeric Hole-Transporting Materials: Influence of Thiophene and Alkyl Chain on Power Conversion Efficiency. Journal of Physical Chemistry C, 2019, 123, 8560-8568.	3.1	18
69	<i>In situ</i> cadmium surface passivation of perovskite nanocrystals for blue LEDs. Journal of Materials Chemistry A, 2021, 9, 26750-26757.	10.3	18
70	Bulk Heterojunction-Assisted Grain Growth for Controllable and Highly Crystalline Perovskite Films. ACS Applied Materials & Interfaces, 2018, 10, 31366-31373.	8.0	17
71	NUV light induced visible emission in Er <sup>3+</sup> â€activated NaSrLa(MoO <sub>4</sub> )O <sub>3</sub> phosphors for green LEDs and thermometer. Journal of the American Ceramic Society, 2020, 103, 1174-1186.	3.8	17
72	Enhanced efficiency of bilayer polymer solar cells by the solvent treatment method. Synthetic Metals, 2015, 199, 408-412.	3.9	16

#	Article	IF	CITATIONS
73	Conjugated polymers containing pyrimidine with electron withdrawing substituents for organic photovoltaics with high open-circuit voltage. Polymer, 2016, 83, 50-58.	3.8	16
74	Dual-Mode Manipulating Multicenter Photoluminescence in a Single-Phased Ba9Lu2Si6O24:Bi3+, Eu3+ Phosphor to Realize White Light/Tunable Emissions. Scientific Reports, 2017, 7, 15884.	3.3	16
75	Wide range yellow emission Sr8MgLa(PO4)7: Eu2+, Mn2+, Tb3+ phosphors for near ultraviolet white LEDs. Materials Research Bulletin, 2018, 107, 280-285.	5.2	16
76	Luminescence properties and energy transfer of Mn4+-doped double perovskite La2ZnTiO6 phosphor. Optical Materials, 2020, 106, 109980.	3.6	16
77	Synthesis and properties of various PPV derivatives with phenyl substituents. Polymer, 2008, 49, 4559-4568.	3.8	15
78	Property modulation of dithienosilole-based polymers via the incorporation of structural isomers of imide- and lactam-functionalized pyrrolo[3,4-c]pyrrole units for polymer solar cells. Polymer, 2015, 65, 243-252.	3.8	15
79	Efficient pyrrolo[3,4-c]pyrrole-1,3-dione-based wide band gap polymer for high-efficiency binary and ternary solar cells. Polymer, 2017, 125, 182-189.	3.8	15
80	Molecular aggregation method for perovskite–fullerene bulk heterostructure solar cells. Journal of Materials Chemistry A, 2020, 8, 1326-1334.	10.3	15
81	A polymer/small-molecule binary-blend hole transport layer for enhancing charge balance in blue perovskite light emitting diodes. Journal of Materials Chemistry A, 2022, 10, 13928-13935.	10.3	15
82	Palladium-Assisted Reaction of 2,2-Dialkylbenzimidazole and Its Implication on Organic Solar Cell Performances. Journal of Physical Chemistry C, 2015, 119, 14063-14075.	3.1	14
83	Luminescence and energy transfer in a color tunable CaY <sub>4</sub> (SiO <sub>4</sub> ) <sub>3</sub> O:Ce <sup>3+</sup> , Mn <sup>2+</sup> , Tb <sup>3+</sup> phosphor for application in white LEDs. RSC Advances, 2016, 6, 79317-79324.	3.6	14
84	Effects of the incorporation of an additional pyrrolo[3,4-c]pyrrole-1,3-dione unit on the repeating unit of highly efficient large band gap polymers containing benzodithiophene and pyrrolo[3,4-c]pyrrole-1,3-dione derivatives. Organic Electronics, 2016, 30, 253-264.	2.6	14
85	Dual-functional light-emitting perovskite solar cells enabled by soft-covered annealing process. Nano Energy, 2019, 61, 251-258.	16.0	14
86	Luminescence and Energy Transfer Process in YNbO <sub>4</sub> :Bi <sup>3</sup> <sup>+</sup> , Sm <sup>3</sup> <sup>+</sup> Phosphors. Science of Advanced Materials, 2017, 9, 349-352.	0.7	14
87	A novel conjugated polymer based on cyclopenta[def]phenanthrene backbone with spiro group. Polymer, 2008, 49, 5643-5649.	3.8	13
88	Synthesis and photoluminescence of novel 3D flower-like CaMoO4 architectures hierarchically self-assembled with tetragonal bipyramid nanocrystals. Optical Materials, 2015, 43, 10-17.	3.6	13
89	6-(2-Thienyl)-4H-thieno[3,2-b]indole based conjugated polymers with low bandgaps for organic solar cells. Synthetic Metals, 2016, 213, 25-33.	3.9	13
90	Side-chain influences on the properties of benzodithiophene-alt-di(thiophen-2-yl)quinoxaline polymers for fullerene-free organic solar cells. Polymer, 2019, 172, 305-311.	3.8	13

#	Article	IF	CITATIONS
91	The biopolymer-assisted synthesis of assembled g-C <sub>3</sub> N <sub>4</sub> open frameworks with electron delocalization channels for prompt H <sub>2</sub> production. Catalysis Science and Technology, 2022, 12, 1368-1377.	4.1	13
92	Crystal structure and two types of Eu3+-centered emission in Eu3+ doped Ca2V2O7. Journal of Luminescence, 2015, 161, 318-322.	3.1	12
93	Benzodithiopheneâ€Based Broad Absorbing Random Copolymers Incorporating Weak and Strong Electron Accepting Imide and Lactam Functionalized Pyrrolo[3,4â€ɛ]pyrrole Derivatives for Polymer Solar Cells. Macromolecular Chemistry and Physics, 2015, 216, 996-1007.	2.2	12
94	Tuning the physical properties of pyrrolo[3,4-c]pyrrole-1,3-dione-based highly efficient large band gap polymers via the chemical modification on the polymer backbone for polymer solar cells. RSC Advances, 2015, 5, 99217-99227.	3.6	12
95	Key chemical parameters related to the width of the charge transfer band and the emission intensity of 5D0→7F2 in Eu3+ doped Ln2O3. Journal of Alloys and Compounds, 2015, 620, 324-328.	5.5	12
96	Effect of La3+ ion doping on the performance of Eu2+ ions in novel Sr3CeNa(PO4)2SiO4 phosphors. Journal of Alloys and Compounds, 2017, 724, 763-773.	5.5	12
97	Ca9Na1/3M2(1-)/3(PO4)7:2x/3Eu3+ (M = Gd, Y): A promising red-emitting phosphor without concentration quenching for optical display applications. Journal of Luminescence, 2018, 194, 346-352.	3.1	12
98	Curvature effects of electron-donating polymers on the device performance of non-fullerene organic solar cells. Journal of Power Sources, 2021, 482, 229045.	7.8	12
99	Syntheses and Characterization of Alkoxyphenyl-Substituted PCPP with Stabilized Blue Emission and Its Derivatives with Ketone Unit in the Main Chain. Macromolecules, 2008, 41, 8324-8331.	4.8	11
100	Efficiency enhancement in polymer optoelectronic devices by introducing titanium sub-oxide layer. Current Applied Physics, 2010, 10, S528-S531.	2.4	11
101	Regioselective 1,2,3-bisazfulleroid: doubly N-bridged bisimino-PCBMs for polymer solar cells. Journal of Materials Chemistry, 2012, 22, 22958.	6.7	11
102	Enhanced photovoltaic performances of bis(pyrrolo[3,4-c]pyrrole-1,3-dione)-based wide band gap polymer via the incorporation of an appropriate spacer unit between pyrrolo[3,4-c]pyrrole-1,3-dione units. Organic Electronics, 2017, 42, 34-41.	2.6	11
103	Tunable up-conversion luminescence from Er3+/Tm3+/Yb3+ tri-doped Sr2CeO4 phosphors. Journal of Luminescence, 2017, 182, 240-245.	3.1	11
104	Full-color tuning in europium doped phosphosilicate phosphors via adjusting crystal field modulation or excitation wavelength. Journal of Alloys and Compounds, 2019, 770, 411-418.	5.5	11
105	Ce 3+ /Tb 3+ â€coactived NaMgBO 3 phosphors toward versatile applications in white LED, FED, and optical antiâ€counterfeiting. Journal of the American Ceramic Society, 2021, 104, 5086-5098.	3.8	11
106	Anthradithiophene–thiophene copolymers with broad UV–vis absorption for organic solar cells and fieldâ€effect transistors. Journal of Polymer Science Part A, 2012, 50, 4119-4126.	2.3	10
107	Effects of the incorporation of bithiophene instead of thiophene between the pyrrolo[3,4-c]pyrrole-1,3-dione units of a bis(pyrrolo[3,4-c]pyrrole-1,3-dione)-based polymer for polymer solar cells. New Journal of Chemistry, 2016, 40, 10153-10160.	2.8	10
108	Full-color tuning by controlling the substitution of cations in europium doped Sr8-xLa2+x(PO4)6-x(SiO4) xO2 phosphors. Dyes and Pigments, 2019, 160, 145-150.	3.7	10

#	Article	IF	CITATIONS
109	Solution-processable ambipolar organic field-effect transistors with bilayer transport channels. Polymer Journal, 2020, 52, 581-588.	2.7	10
110	Enhanced Charge Separation in Ternary Bulk-Heterojunction Organic Solar Cells by Fullerenes. Journal of Physical Chemistry Letters, 2021, 12, 6418-6424.	4.6	10
111	Novel conjugated polymers employing the binding of polyfluorene derivatives and C60. Synthetic Metals, 2009, 159, 1529-1537.	3.9	9
112	Synthesis and characterization of low-bandgap copolymers based on dihexyl-2H-benzimidazole and terthiophene. Synthetic Metals, 2010, 160, 2618-2622.	3.9	9
113	Highly transparent polymer light-emitting diode using modified aluminum-doped zinc oxide top electrode. Applied Physics Letters, 2012, 100, 133306.	3.3	9
114	Pyrrolo[3,4-c]pyrrole-1,3-dione-based large band gap polymers containing benzodithiophene derivatives for highly efficient simple structured polymer solar cells. Journal of Polymer Science Part A, 2014, 52, n/a-n/a.	2.3	9
115	Thiophene and thieno[3,2-b]thiophene π-bridged pyrrolo[3,4-c]pyrrole-1,3-dione-based wide band-gap polymers for fullerene and non-fullerene organic solar cells. Organic Electronics, 2018, 63, 78-85.	2.6	9
116	Influence of thiophene and furan π–bridge on the properties of poly(benzodithiophene-alt-bis(π–bridge)pyrrolopyrrole-1,3-dione) for organic solar cell applications. Polymer, 2021, 229, 123991.	3.8	9
117	Modulation of the properties of pyrrolo[3,4-c]pyrrole-1,4-dione based polymers containing 2,5-di(2-thienyl)pyrrole derivatives with different substitutions on the pyrrole unit. New Journal of Chemistry, 2015, 39, 4658-4669.	2.8	8
118	Photocurrent enhancement of an efficient large band gap polymer incorporating benzodithiophene and weak electron accepting pyrrolo[3,4â^'c]pyrroleâ^'1,3â^'dione derivatives via the insertion of a strong electron accepting thieno[3,4â^'b]thiophene unit. Polymer, 2015, 80, 95-103.	3.8	8
119	Benzodithiophene based ternary copolymer containing covalently bonded pyrrolo[3,4-c]pyrrole-1,3-dione and benzothiadiazole for efficient polymer solar cells utilizing high energy sunlight. Organic Electronics, 2016, 38, 283-291.	2.6	8
120	Synchronized-pressing fabrication of cost-efficient crystalline perovskite solar cells <i>via</i> intermediate engineering. Nanoscale, 2018, 10, 9628-9633.	5.6	8
121	Photovoltaic polymers based on difluoroqinoxaline units with deep <scp>HOMO</scp> levels. Journal of Polymer Science Part A, 2018, 56, 1489-1497.	2.3	8
122	Enhanced Magnetic Properties of FeCo Alloys by Two-Step Electroless Plating. Journal of the Electrochemical Society, 2019, 166, D131-D136.	2.9	8
123	Rational design of efficient near-infrared photon conversion channel via dual-upconversion process for superior photocatalyst. Carbon, 2020, 169, 111-117.	10.3	8
124	Theoretical design and characterization of high efficient Sr9Ln(PO4)7: Eu2+ phosphors. Materials Research Bulletin, 2020, 127, 110856.	5.2	8
125	Self-reduction process of Eu3+ to Eu2+ in Eu-doped SrLaMgTaO6 double perovskite thin films and its photoluminescence properties. Optical Materials, 2021, 116, 111092.	3.6	8
126	Flexible light-emitting three-terminal device with color-controlled emission. Organic Electronics, 2009, 10, 426-431.	2.6	7

#	Article	IF	CITATIONS
127	Syntheses and characterization of new low-band gap polymers containing 4H-cyclopenta[def]phenanthrene unit and 4,7-di(thien-2-yl)-2H-benzimidazole-2-spirocyclohexane for photovoltaic device. Synthetic Metals, 2011, 161, 1336-1342.	3.9	7
128	Synthesis and characterization of dimethyl-benzimidazole based low bandgap copolymers for OPVs. Synthetic Metals, 2012, 162, 988-994.	3.9	7
129	Syntheses of pyrimidineâ€based polymers containing electronâ€withdrawing substituent with high open circuit voltage and applications for polymer solar cells. Journal of Polymer Science Part A, 2016, 54, 771-784.	2.3	7
130	Property modulation of ternary copolymer via the diverse arrangements of two different repeating units for polymer solar cells and thin film transistors. Polymer, 2016, 95, 18-25.	3.8	7
131	Enhanced efficiency and stability of polymer solar cells using solution-processed nickel oxide as hole transport material. Current Applied Physics, 2017, 17, 1232-1237.	2.4	7
132	Improved exciton dissociation efficiency by a carbon-quantum-dot doped workfunction modifying layer in polymer solar cells. Current Applied Physics, 2021, 21, 140-146.	2.4	7
133	Water-Repellent Perovskites Induced by a Blend of Organic Halide Salts for Efficient and Stable Solar Cells. ACS Applied Materials & Interfaces, 2021, 13, 33172-33181.	8.0	7
134	Synthesis and characterization of 2H-benzimidazole- and terthiophene-based polymer for organic photovoltaics. Synthetic Metals, 2011, 161, 307-312.	3.9	6
135	Increasing of stability depended on the position of alkoxy group in PPV. Synthetic Metals, 2011, 161, 1186-1193.	3.9	6
136	PyrroleN-alkyl side chain effects on the properties of pyrrolo[3,4-c]pyrrole-1,3-dione-based polymers for polymer solar cells. New Journal of Chemistry, 2018, 42, 12045-12053.	2.8	6
137	Cation substitution induced excellent quantum efficiency and thermal stability in (Ca1â^'xSrx)9La(PO4)7:Eu2+ phosphors. New Journal of Chemistry, 2019, 43, 12325-12330.	2.8	6
138	Efficient Polymeric Donor for Both Visible and Near-Infrared-Absorbing Organic Solar Cells. ACS Applied Energy Materials, 2019, 2, 4284-4291.	5.1	6
139	Kerf-Less Exfoliated Thin Silicon Wafer Prepared by Nickel Electrodeposition for Solar Cells. Frontiers in Chemistry, 2018, 6, 600.	3.6	6
140	Effects of replacing benzodithiophene with a benzothiadiazole derivative on an efficient wide band-gap benzodithiophene-alt-pyrrolo[3,4-c]pyrrole-1,3(2H,5H)-dione copolymer. Journal of Photochemistry and Photobiology A: Chemistry, 2019, 368, 162-167.	3.9	6
141	Water-stable polymer hole transport layer in organic and perovskite light-emitting diodes. Journal of Power Sources, 2020, 478, 228810.	7.8	6
142	Enhanced performance of ternary polymer solar cells via property modulation of co-absorbing wide band-gap polymers. Journal of Power Sources, 2020, 471, 228457.	7.8	6
143	Enhanced photovoltaic performance of benzodithiophene-alt-bis(thiophen-2-yl)quinoxaline polymers via ï€â€"bridge engineering for non-fullerene organic solar cells. Polymer, 2020, 194, 122408.	3.8	6
144	Carrier losses in non-geminate charge-transferred states of nonfullerene acceptor-based organic solar cells. Spectrochimica Acta - Part A: Molecular and Biomolecular Spectroscopy, 2021, 250, 119227.	3.9	6

#	Article	IF	CITATIONS
145	Enhancement in charge extraction and moisture stability of perovskite solar cell via infiltration of charge transport material in grain boundaries. Journal of Power Sources, 2021, 506, 230212.	7.8	6
146	Synthesis and characterization of polycyclopentaphenanthrene with carbazole or oxidiazole pendant units. Polymer Journal, 2012, 44, 347-352.	2.7	5
147	Synthesis and characterization of phenathrothiadiazole-based conjugated polymer for photovoltaic device. Synthetic Metals, 2012, 162, 1936-1943.	3.9	5
148	Simultaneous realization of two approaches to white light in single-component phosphors. Optics Express, 2014, 22, 25500.	3.4	5
149	Elaboration, Structure and Luminescence of Sphere-Like CaF2:RE Sub-Microparticles by Ionic Liquids Based Hydrothermal Process. Journal of Nanoscience and Nanotechnology, 2016, 16, 1146-1150.	0.9	5
150	Successful incorporation of optical spacer and additive solvent for enhancing the photocurrent of polymer solar cell. Solar Energy Materials and Solar Cells, 2016, 153, 131-137.	6.2	5
151	Effects of inserting keto-functionalized side-chains instead of imide-functionalized side-chain on the pyrrole backbone of 2,5-bis(2-thienyl)pyrrole-based polymers for organic solar cells. Journal of Photochemistry and Photobiology A: Chemistry, 2019, 371, 387-394.	3.9	5
152	Synthesis and Photovoltaic Properties of Quinoxaline-Based Semiconducting Polymers with Fluoro Atoms. Bulletin of the Korean Chemical Society, 2014, 35, 2245-2250.	1.9	5
153	Imide-linked alkyl chain influence on the properties of pyrrole-based imide-functionalized polymers containing pyrrolo[3,4-c]pyrrole-1,3(2H,5H)-dione and benzodithiophene units for polymer solar cells. Synthetic Metals, 2016, 220, 34-40.	3.9	4
154	Regioregular dithienosilole- and dithienogermole-based small molecules with symmetric distal/distal orientation of F atoms. Dyes and Pigments, 2018, 155, 7-13.	3.7	4
155	Controllable Eu valence based on linear structural evolution in single-phased Sr3-La1+(PO4)3-(SiO4) phosphors to realize tunable/white light emissions. Journal of Alloys and Compounds, 2020, 817, 152743.	5.5	4
156	Pyrrolo[3,4-c]pyrrole-1,3-dione Based Wide Band Gap Polymers for Polymer Solar Cells. Journal of Nanoscience and Nanotechnology, 2017, 17, 5556-5561.	0.9	4
157	Substituent position-induced color tunability in polymer light-emitting diodes. Applied Physics Letters, 2002, 81, 1732-1734.	3.3	3
158	Switchable polarity in polymer solar cells using conjugated polyelectrolyte. Synthetic Metals, 2014, 188, 1-5.	3.9	3
159	Synthesis and Properties of Copolymer with Carbazole and F-Quinoxaline Units for OPVs. Molecular Crystals and Liquid Crystals, 2015, 620, 100-106.	0.9	3
160	Opto-electrical, charge transport and photovoltaic property modulation of 2,5-di(2-thienyl)pyrrole-based polymers via the incorporation of alkyl, aryl and cyano groups on the pyrrole unit. Polymer Bulletin, 2015, 72, 1899-1919.	3.3	3
161	Photoluminescence properties of SrLaMgTaO6 double-perovskite thin film. Journal of Alloys and Compounds, 2018, 755, 67-72.	5.5	3
162	Two new tercopolymers incorporating electron-rich benzodithiophene and electron-accepting pyrrolo[3,4-c]pyrrole-1,3-dione and difluorobenzothiadiazole derivatives for polymer solar cells. Polymer Bulletin, 2018, 75, 239-253.	3.3	3

#	Article	IF	CITATIONS
163	Gate-enhanced photocurrent of (6,5) single-walled carbon nanotube based field effect transistor. Carbon, 2018, 139, 709-715.	10.3	3
164	Syntheses and Properties of Random Copolymers Using Thienyl-Thieno-Indole and Bithiophene-Dicarboximide with Different Ratios. Macromolecular Research, 2019, 27, 470-475.	2.4	3
165	Synthesis and Photovoltaic Properties of Copolymer Containing Fused Donor and Difluoroquinoxaline Moieties. Bulletin of the Korean Chemical Society, 2014, 35, 2963-2968.	1.9	3
166	Enhanced phase separation in PEDOT:PSS hole transport layer by introducing phenylethylammonium iodide for efficient perovskite solar cells. Journal of Renewable and Sustainable Energy, 2022, 14, 013502.	2.0	3
167	Up-conversion luminescence performance of Tm3+/Yb3+ co-doped strontium cerate phosphors. Optik, 2022, 262, 169264.	2.9	3
168	Synthesis and properties of thiophene- and quinoxaline-based random copolymers for organic photovoltaics. Polymer Bulletin, 2017, 74, 2755-2766.	3.3	2
169	Wide band-gap organic molecules containing benzodithiophene and difluoroquinoxaline derivatives for solar cell applications. Molecular Crystals and Liquid Crystals, 2019, 685, 29-39.	0.9	2
170	Visible to Nearâ€Infraredâ€Absorbing Polymers Containing Bithiazole and 2,3â€Didodecylâ€6,7â€Difluoroquinoxaline Derivatives for Polymer Solar Cells. Bulletin of the Korean Chemical Society, 2019, 40, 686-690.	1.9	2
171	Improved Adhesion of Metal Electrode Layer on Si <sub>3</sub> N <sub>4</sub> Substrate through an All-Wet Process. ECS Journal of Solid State Science and Technology, 2019, 8, P159-P164.	1.8	2
172	Fluorescence spectroscopy-based study of balanced transport of charge carriers in hot-air-annealed perovskites. Spectrochimica Acta - Part A: Molecular and Biomolecular Spectroscopy, 2019, 207, 68-72.	3.9	2
173	Synthesis and properties of mono―and diâ€fluoroâ€substituted 2,3â€didodecylquinoxalineâ€based polymers for polymer solar cells. Journal of Polymer Science Part A, 2019, 57, 545-552.	2.3	2
174	Design and theoretical study of superlative quantum efficiency and thermal stability phosphor: The system of Sr9Eu(PO4)7. Journal of Alloys and Compounds, 2021, 862, 158285.	5.5	2
175	Versatile control of concentration gradients in non-fullerene acceptor-based bulk heterojunction films using solvent rinse treatments. Green Energy and Environment, 2021, , .	8.7	2
176	Photovoltaic Performances of Dye-Sensitized Solar Cells Based on Modified Polybutadiene Matrix Electrolytes by Sol-Gel Process. Polymers, 2022, 14, 2347.	4.5	2
177	Novel Electroluminescent PPV Copolymers Containing Si-phenyl and Difluorovinylene Units. Polymer Journal, 2008, 40, 965-970.	2.7	1
178	Color stability of conjugated polymer with difluoro groups in vinylene units. Macromolecular Research, 2011, 19, 753-756.	2.4	1
179	Structural, vibrational and band gap tunability of lead-free (1Ââ^'Âx)NaBiTO3–xBiMnO3 ceramics. Journal of Materials Science: Materials in Electronics, 2017, 28, 18508-18514.	2.2	1
180	Synthesis and photovoltaic properties of organic molecules based on difluoroquinoxaline derivatives for OPVs. Molecular Crystals and Liquid Crystals, 2020, 705, 57-64.	0.9	1

#	Article	IF	CITATIONS
181	Synthesis and Characterization of Novel D-A Conjugated Polymers Based on Fluorinated Quinoxaline and Thiophene Series for Polymer Solar Cells. Journal of Nanoscience and Nanotechnology, 2017, 17, 5802-5805.	0.9	1
182	The Effect of Charge Compensation on the Luminescence Behavior of Eu <sup>3+</sup> -Doped Perovskite CaZrO <sub>3</sub> Red Phosphor. Nanoscience and Nanotechnology Letters, 2018, 10, 703-708.	0.4	1
183	Correlation Between Lateral Photovoltaic Effect and Conductivity in p-type Silicon Substrates. Bulletin of the Korean Chemical Society, 2013, 34, 1845-1847.	1.9	1
184	Design and photovoltaic properties of conjugated polymers based on quinoxaline and diketopyrrolopyrrole for OSCs. Synthetic Metals, 2022, 285, 117016.	3.9	1
185	Effective methods for improving device performances of P-I-N perovskite solar cells. , 2017, , .		0
186	Synthesis of Alkylâ€Substituted Quinoxalineâ€Based Copolymers Along with Photophysical Property Modulation for Polymer Solar Cells. Macromolecular Chemistry and Physics, 2018, 219, 1800117.	2.2	0
187	Design and synthesis of small molecules with difluoroquinoxaline units for OSCs. Molecular Crystals and Liquid Crystals, 2020, 705, 79-86.	0.9	0
188	Small molecules based difluoroquinoxaline for organic solar cells. Molecular Crystals and Liquid Crystals, 2021, 728, 45-51.	0.9	0
189	Efficiency Enhancement in Polymer Solar Cell Using Solution-processed Vanadium Oxide Hole Transport Layer. New Physics: Sae Mulli, 2015, 65, 709-714.	0.1	0
190	Study of Solution-processable Bilayer Polymer Solar Cells. New Physics: Sae Mulli, 2015, 65, 741-746.	0.1	0
191	Synthesis and Photovoltaic Properties of Copolymers with Fluorinated Quinoxaline and Fluorene Moiety. Applied Chemistry for Engineering, 2016, 27, 467-471.	0.2	0
192	Enhancement in the Device Performance of an Organic Field-Effect Transistor Through Thermal Annealing. New Physics: Sae Mulli, 2017, 67, 1180-1186.	0.1	0
193	Highly efficient and freely soluble titanium sub-oxide powder as interfacial functional material for versatile photovoltaic cells. Chemical Engineering Journal, 2022, 450, 138017.	12.7	0